Rayleigh Loss Estimation Using One-Dimensional Flow Analysis for LPRE

Sawyer R. Morgan[1] and Roy J. Hartfield Jr.[2]
Department of Aerospace Engineering, Auburn University, Auburn, Alabama, 36832

Rayleigh losses in combustion chambers are traditionally estimated using empirical correlations to approximate the compressibility effects of heat addition in high-speed reacting flows. This work presents an analytical evaluation of Rayleigh stagnation pressure losses and quantifies their performance impact in a liquid-propellant rocket engine. A quasi-one-dimensional compressible flow model is developed to reconstruct the axial stagnation pressure evolution through the combustion chamber and nozzle. This framework enables direct computation of stagnation pressure decay as a function of total temperature rise in the combustion chamber, allowing systematic parametric sweeps over operating conditions for a fixed engine geometry. Performance impacts are quantified through variations in thrust and specific impulse relative to an ideal, constant stagnation pressure baseline. Results demonstrate a monotonic decrease in engine performance with increasing total temperature rise due to Rayleigh total pressure losses. The model is computationally efficient and suitable for early-stage design trade studies. Validation against NASA Chemical Equilibrium with Applications shows good agreement in exit pressure and performance metrics, supporting the utility of the approach for rapid internal ballistics assessment.

I. Nomenclature

Variables

M	=	Mach number
s	=	entropy
γ	=	ratio of specific heats
W	=	molecular weight
R	=	gas constant
T	=	temperature
P	=	pressure
A	=	cross-sectional area
x	=	axial coordinate
G	=	forcing function
$\dot{m}$	=	mass flow rate
V	=	velocity
F	=	thrust
$\mathcal{L}$	=	loss metric
c_p	=	specific heat at constant pressure
I_{sp}	=	specific impulse
g_0	=	acceleration of gravity at sea level
P_a	=	atmospheric pressure at sea level
R_u	=	universal gas constant

Subscripts

0	=	stagnation property
Q	=	heat transfer
A	=	area variation
f	=	friction
e	=	nozzle exit
inj	=	chamber injection face
ns	=	chamber endpoint, nozzle entry
ref	=	ideal reference solution
R	=	Rayleigh loss solution

[1] Undergraduate, Research Assistant, Department of Aerospace Engineering, AIAA Student Member, 1923879
[2] Professor, Department of Aerospace Engineering, Associate Fellow, 076983

II. Introduction

Liquid Propellant Rocket Engine (LPRE) performance is governed by the thermodynamic evolution of compressible flow through the combustion chamber and nozzle [1]. Heat addition, area variation, and friction collectively influence the stagnation properties of the flow, which directly determines thrust and specific impulse [2]. Accurate prediction of stagnation pressure evolution is therefore essential for reliable performance estimation during the conceptual design phase. Rayleigh flow describes the behavior of compressible flow with heat addition in a constant area duct [3]. In this regime, thermal energy addition drives the flow toward sonic conditions while simultaneously reducing available stagnation pressure. In LPREs, combustion within the chamber introduces substantial heat addition prior to nozzle expansion. As a result, stagnation pressure losses occur upstream of the nozzle and directly impact available expansion work. While nozzle losses are typically associated with friction and efficiency factors, Rayleigh losses originate within the combustion chamber and represent a distinct thermodynamic penalty.

In early-stage design, Rayleigh losses are often approximated using empirical correlations or incorporated into lumped loss coefficients. High-fidelity computational approaches can capture these effects but are typically computationally expensive. The absence of a fast analytical framework for reconstructing stagnation pressure evolution limits the ability to perform rapid trade studies and sensitivity analyses. The objective of this work is to develop a computationally efficient quasi-one-dimensional model that reconstructs the axial stagnation pressure distribution of an LPRE and isolates Rayleigh total pressure losses due solely to heat addition. Friction is retained in the Mach number solution to preserve realistic flow evolution, but entropy reconstruction excludes frictional contributions to quantify stagnation pressure decay due to heat addition independently.

A parametric sweep over combustion chamber total temperature rise is performed for a fixed engine geometry. Performance impacts are quantified through changes in thrust and specific impulse relative to an ideal solution with no stagnation pressure degradation. Model predictions are validated against NASA Chemical Equilibrium with Applications (CEA) [4], demonstrating good agreement in exit pressure and performance trends.

III. Methodology

A. Quasi-One-Dimensional Formulation

A quasi-one-dimensional flow solution was implemented to model the flow field of an LPRE thrust chamber. The model, described graphically in Fig. 1, assumes steady, single-phase flow, locally one-dimensional velocity, and axis-symmetric geometry.

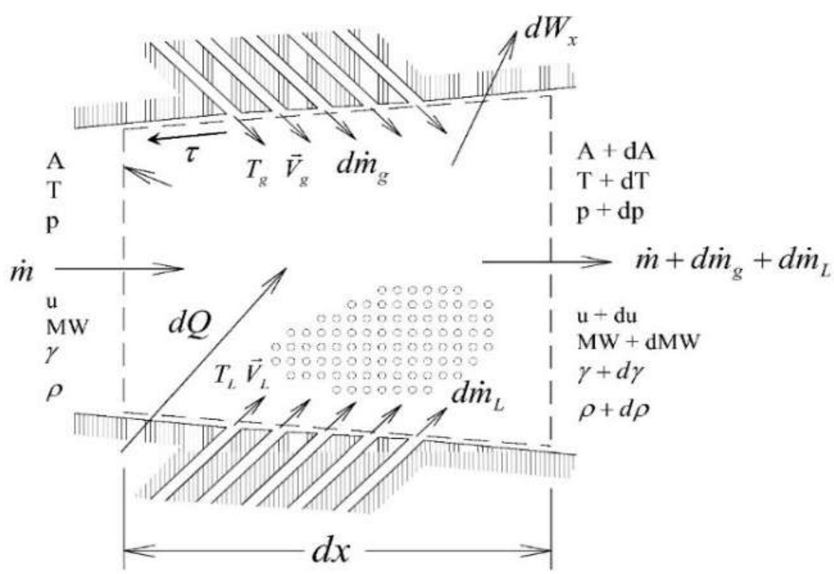

Fig. 1 Differential control volume formulation used to derive the quasi-one-dimensional governing equations

The infinitesimal element of length dx accounts for axial variations in flow area, pressure, temperature, velocity, density, specific heat ratio, and molecular weight. The model incorporates wall heat addition, shear stress effects, distributed mass addition from propellant injection, and liquid-phase mass transfer. Following the influence-coefficient framework presented by Shapiro [5], applications of conservation of mass, momentum, and energy yield the quasi-one-dimensional compressible flow formulation used to reconstruct the internal ballistics and stagnation pressure evolution of the LPRE.

In differential form, the principal governing equation may be expressed as:

$$\frac{\mathrm{d}M^2}{\mathrm{d}x} = \frac{M^2\left(1 + \frac{\gamma(x) - 1}{2}M^2\right)}{\left(1 - M^2\right)} \cdot G\left(x, M^2\right) \tag{1}$$

The right-hand side is naturally separated into two components, a factor term which contains singularity behavior at a Mach number of 1, and a general forcing function that accounts for property variation in the combustion chamber and nozzle. This decomposition isolates the sonic singularity and facilitates the numerical identification of the sonic point while preserving physical interpretability of the forcing mechanisms. The generalized forcing function is written as:

$$G\left(x, M^2\right) = G_Q + G_A + G_f \tag{2}$$

The term G_Q contains the physical effect of Rayleigh heat addition in the combustion chamber and describes the influence of total temperature on the flow field. The stagnation temperature increase associated with combustion was modeled using a tangent function to ensure continuous derivatives for numerical stability. A scaling parameter was introduced to vary the magnitude of total temperature rise, enabling systematic evaluation of Rayleigh-induced stagnation pressure losses. The geometric term G_A accounts for axial variation in flow area variation. The thrust chamber geometry prescribed as a smooth, piecewise function of axial position, consisting of a constant-area combustion chamber followed by a converging-diverging nozzle. A throat area of 0.672 m² and an expansion ratio of 16 were selected to represent an F-1-class configuration. The combustion chamber length was fixed at 0.5 m, with a total thrust chamber length of 3.35 m. This geometry was held constant for all parametric cases. The friction term G_f models viscous momentum losses along the chamber wall. A fanning friction factor formulation was employed, with spatial variation introduced through the local hydraulic diameter corresponding to the prescribed area distribution. Figure 2 displays the prescribed inputs used for the model.

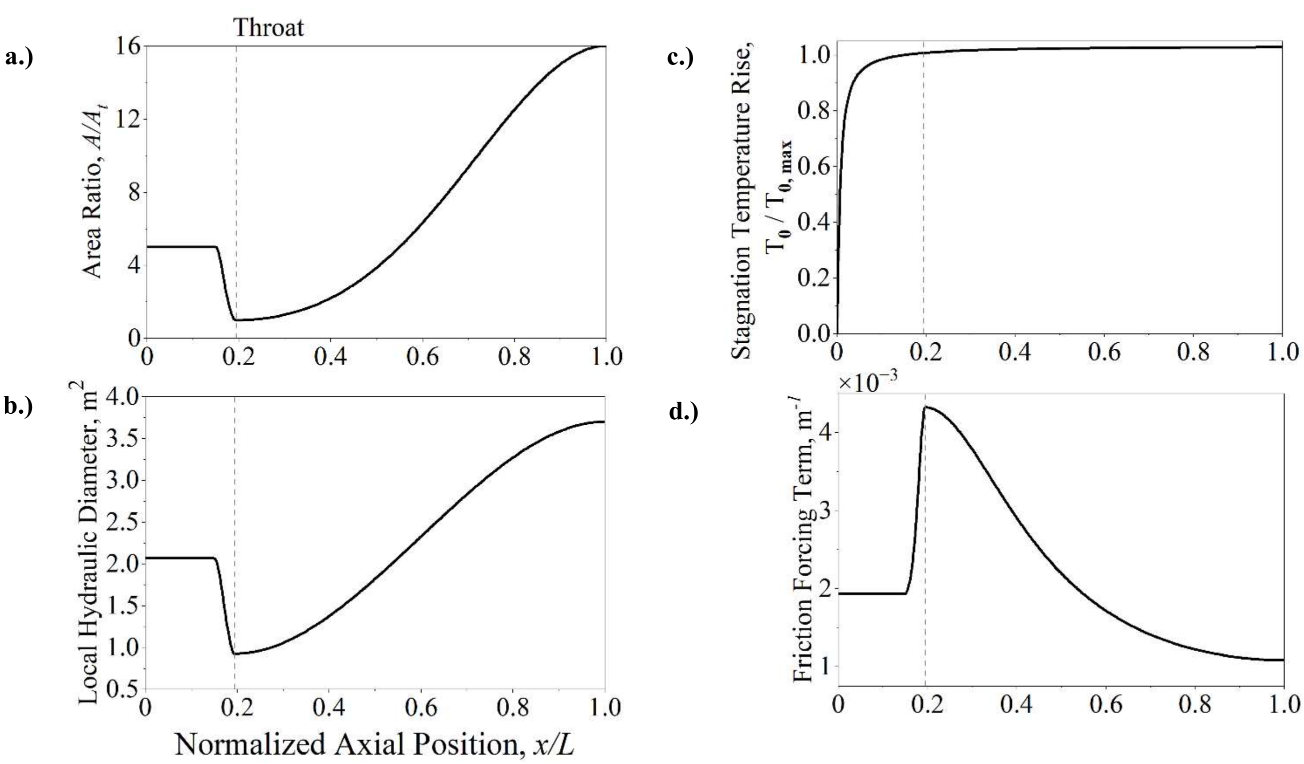

Fig. 2. Prescribed geometric, thermal, and frictional inputs to the quasi-one-dimensional model: normalized area distribution (Panel a.), normalized stagnation temperature rise (Panel b.), local hydraulic diameter (Panel c.), and friction forcing term (Panel d.), plotted versus normalized axial position.

B. Thermodynamic Property Modeling and Fixed-Point Iteration

At the high temperatures reached in the combustion chamber, both the ratio of specific heats and the molecular weight of the propellant mixture vary significantly with temperature [6]. Assuming calorically perfect behavior would therefore introduce non-negligible error [7]. To account for this effect, the liquid oxygen and RP-1 propellant combination was modeled using temperature-dependent specific heats and molecular weight.

Thermodynamic data were extracted from NASA CEA at a fixed mixture ratio of 2.27 over a range of temperatures representative of the combustion process. Continuous interpolation functions were constructed for the specific heat at constant pressure and the mixture molecular weight,

$$c_p = c_p(T), \qquad W = W(T) \tag{3,4}$$

The gas constant of the mixture and the ratio of specific heats were obtained from their respective defining relations:

$$R(T) = \frac{R_u}{W(T)}, \qquad \gamma(T) = \frac{c_p(T)}{c_p(T) - R(T)} \tag{5,6}$$

The thermodynamic properties depend on the local static temperature, which is reconstructed from the axial Mach number solution using the relation:

$$T(x) = \frac{T_0(x)}{1 + \frac{\gamma(x) - 1}{2} M^2(x)} \tag{7}$$

However, the Mach number distribution itself depends on the temperature-dependent specific heat ratio appearing in Eq. (6), resulting in a coupled system between flow and thermodynamic properties [8]. To resolve this coupling, a fixed-point iteration was employed. An initial estimate of γ was obtained by interpolating properties from the prescribed total temperature profile. Equation (1) was then integrated to obtain Mach number, from which the static temperature is reconstructed by Eq. (7). The temperature-dependent properties were subsequently updated using Eqs. (3) and (4), and the process was repeated until the change in γ between successive iterations satisfied a prescribed convergence tolerance.

B. Numerical Integration Procedure

The governing Mach number equation, Eq. (1), was integrated as a first order ordinary differential equation in the axial coordinate using a fourth-order Runge-Kutta scheme with uniform spatial discretization. The solution was constructed by performing separate integrations upstream and downstream of the sonic point, corresponding to the supersonic and subsonic branches of the flow, respectively.

The factor term in Eq. (1) contains a singularity at Mach 1. The sonic location was determined by computing the root of the forcing function over the axial domain. To obtain the limiting slope at the sonic point, L'Hôpital's Rule was applied on the right-hand side of equation (1). This limiting slope was used to initiate the integration on both sides of the sonic point, ensuring continuity of the Mach number distribution and selection of the physically admissible solution branch.

This integration was coupled to the thermodynamic fixed-point iteration described previously. At each iteration, the Mach number distribution was computed using the current estimate of thermodynamic properties, from which the static temperature was reconstructed. Updated temperature-dependent properties were then obtained, and the process was repeated until the change in specific heat ratio between successive iterations satisfied the prescribed convergence tolerance.

To assess numerical stability, grid sensitivity was evaluated by refining the axial discretization until variations in the Mach number and stagnation pressure distributions were negligible. The solution procedure exhibited stable convergence across the full range of total temperature scaling cases considered, and no artificial damping or smoothing was required to maintain numerical stability.

C. Rayleigh Loss Formulation

Rayleigh heat addition associated with combustion generates entropy within the flow. The entropy increase reduces available stagnation pressure and consequently reduces thrust in the LPRE. Entropy generation due to Rayleigh heat addition within the constant-area combustion chamber was evaluated using the thermodynamic relation:

$$\left(\frac{ds}{dx}\right)_Q = \frac{c_p(x)}{T(x)}\left(\frac{dT_0(x)}{dx}\right) \tag{8}$$

Wall-friction effects were included in the flow solution but were excluded from the stagnation pressure reconstruction to isolate heat-addition losses. Entropy was then related to stagnation pressure through:

$$\frac{d\ln\left(P_0(x)\right)}{dx} = \left(\frac{c_p(x)}{R(x)}\right)\left(\frac{dT_0(x)}{T_0(x)}\right) - \left(\frac{1}{R(x)}\frac{ds}{dx}\right) \tag{9}$$

Equation (9) was written in logarithmic derivative form to ensure smooth numerical integration. Stagnation pressure evolution was reconstructed through the combustion chamber using a fourth-order Runge-Kutta integration scheme, consistent with the Mach number solution procedure.

A reference solution was constructed using identical geometry and thermodynamic property treatment. To remove Rayleigh driven effects in the Mach number equation, the heat-addition forcing term in Eq. (2) was set to zero in the reference case. Stagnation pressure remained constant within the combustion chamber for the reference solution. The Rayleigh loss metric was defined as:

$$\mathcal{L}_R = 1 - \frac{P_{0,\,ns}}{P_{0,\,ns,\,ref}} \tag{10}$$

where Eq. (10) was evaluated at the combustion chamber exit for each parametric case, directly quantifying stagnation pressure degradation due to heat addition.

D. Performance Evaluation

Engine performance was evaluated through thrust and specific impulse, computed from the exit conditions predicted by the obtained flow solution. These metrics quantify the impact of Rayleigh stagnation pressure degradation on overall propulsion performance. Sea-level thrust was computed using:

$$F = \dot{m}V_e + \left(P_e - P_a\right)A_e \tag{11}$$

where the exit velocity was obtained through:

$$V_e = M_e\sqrt{\gamma_e R_e T_e} \tag{12}$$

Specific impulse was computed:

$$I_{sp} = \frac{F}{\dot{m}g_0} \tag{13}$$

To quantify the thrust loss due to Rayleigh heat addition, the flow solution was compared to the reference solution. Thrust loss was defined:

$$\mathcal{L}_F = 1 - \frac{F}{F_{ref}} \tag{14}$$

Similarly, specific impulse loss was defined:

$$\mathcal{L}_{I_{sp}} = 1 - \frac{I_{sp}}{I_{sp,\,ref}} \tag{15}$$

These performance metrics enable direct quantification of how Rayleigh-driven stagnation pressure losses propagate to thrust and specific impulse losses.

IV. Results and Discussion

A. Baseline Validation Against NASA CEA and Classical Compressible Flow Theory

To assess predictive accuracy of the quasi-one-dimensional flow solution, a baseline comparison was performed against NASA's CEA rocket solver. The comparison was conducted using identical operating and geometrical parameters, including a chamber pressure of 77.56602 bar, mixture ratio O/F 2.27, nozzle contraction ratio of 5, and supersonic expansion ratio of 16. The CEA rocket solver was executed with the finite combustor option to ensure consistency with the finite length chamber modeled in the present formulation. Under these matched conditions, the predicted nozzle exit static pressure agreed with the CEA solution to within 0.61%. This level of agreement indicates that the reduced order formulation captures the dominant thermodynamic and compressible-flow behavior governing nozzle expansion for the specified operating point. Minor discrepancies are attributed to differences in thermodynamic modeling assumptions and to the formulation. In particular, the present model includes wall friction effects through a prescribed Fanning friction factor, whereas the CEA rocket formulation assumes ideal, one-dimensional expansion. These differences may contribute to the observed 0.61% deviation in exit pressure. This level of agreement demonstrates that the present formulation captures the dominant thermodynamic and compressible-flow behavior governing nozzle expansion while incorporating additional physical effects not represented in the CEA reference solution.

Table I. Exit Pressure Comparison with NASA CEA

Quantity	Present Model, bar	CEA, bar	Percent difference
Exit Pressure	0.5349	0.5317	0.61%

To verify the mathematical consistency of the generalized quasi-one-dimensional formulation, the governing Mach equation was reduced to classical limiting cases by selectively deactivating individual forcing terms. Heat-only, friction-only, and area-only configurations were evaluated under constant thermodynamic properties and compared against the analytical Rayleigh, Fanno, and isentropic relations, respectively [3]. Figure 3 demonstrates that the generalized formulation reduces exactly to the classical Rayleigh, Fanno, and isentropic flow solutions under their respective limiting assumptions.

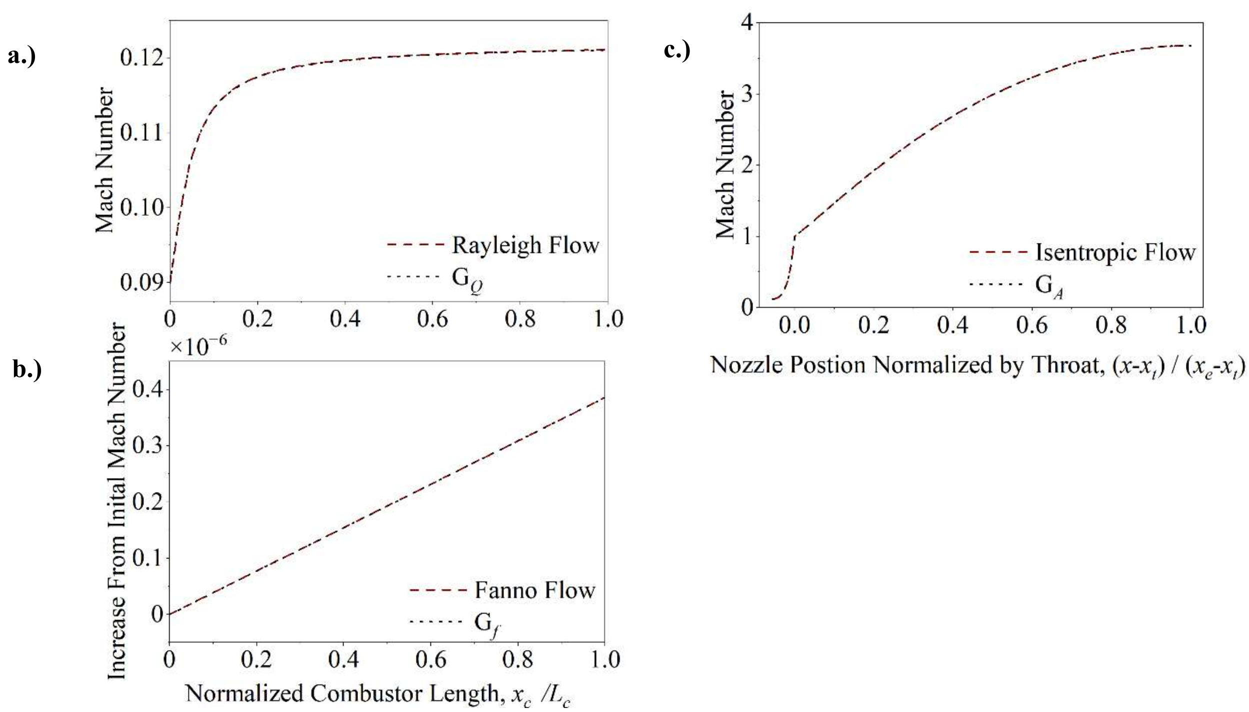

Figure 3. Reduction to classical compressible-flow theory: (a) Rayleigh flow (heat-only, constant area), (b) Fanno flow (friction-only, constant area), and (c) isentropic nozzle flow (area-only, constant thermodynamic properties). Numerical solutions collapse to their corresponding analytical relations in each limiting case.

The generalized Mach formulation exhibits exact collapse to the classical limiting cases when individual forcing terms are isolated. Under heat-only conditions in the constant-area combustor, the solver reproduces the analytical Rayleigh solution, while friction-only forcing yields the classical Fanno evolution. Similarly, when restricted to area variation with constant thermodynamic properties, the nozzle solution aligns precisely with the isentropic area-Mach relation. In each case, the numerical and analytical Mach distributions are indistinguishable within good precision, confirming that the generalized governing equation is algebraically consistent with established compressible-flow theory and that each physical forcing mechanism has been correctly implemented. These comparisons provide a direct assessment of whether the generalized model collapses to established compressible-flow theory when restricted to the assumptions underlying each classical solution.

B. Flow Field Response to Total Temperature Scaling

To examine the influence of total temperature variation on the internal flow structure, the axial Mach number distribution and stagnation pressure profile were computed across the total temperature sweep. Figure 4 presents the resulting Mach number and stagnation temperature profiles.

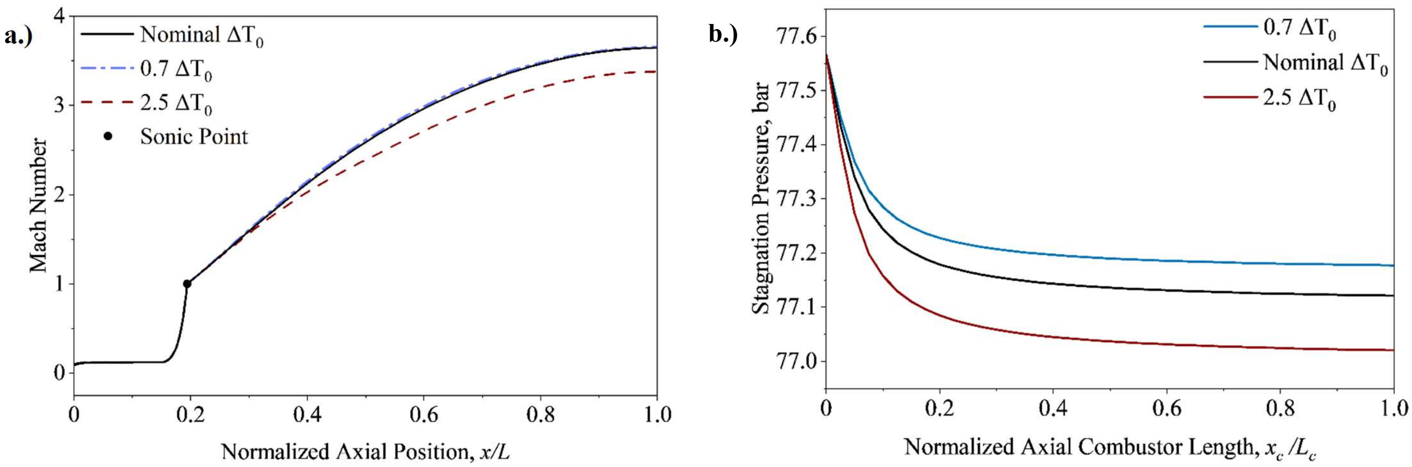

Fig. 4 (a.) Mach Number and (b.) Stagnation Pressure Sensitivity to Total Temperature Scaling

The Mach number profile in the subsonic combustion chamber region remains nearly invariant across the sweep. The weak sensitivity can be attributed to the larger diameter and constant cross-section in the combustor. Deviations emerge downstream of the throat, where the supersonic expansion region displays a decrease in Mach number corresponding to increased total temperature increase in the combustion chamber.

To quantify the stagnation pressure degradation attributed to Rayleigh heat addition within the combustion chamber, the reconstructed stagnation pressure distribution was evaluated for the total temperature scaling cases. All cases share identical geometry and inlet stagnation conditions. Only the imposed total temperature rise within the constant-area chamber is varied.

Across all cases, stagnation pressure decreases monotonically through the constant-area combustion chamber, consistent with entropy generation induced by heat addition. The pressure decay is smooth and continuous, reflecting the cumulative nature of Rayleigh losses rather than a discrete pressure drop. The most rapid stagnation pressure reduction occurs in the upstream region of the chamber, where the imposed total temperature gradient is largest. As the total temperature profile approaches its asymptotic value downstream, the local rate of entropy generation decreases, and the stagnation pressure gradient correspondingly weakens. The smooth, monotonic behavior of the reconstructed profiles confirms numerical stability of the logarithmic integration formulation presented in Section III and indicates that the entropy reconstruction procedure does not introduce artificial oscillations or non-physical behavior.

Increasing total temperature rise intensifies stagnation pressure degradation across the combustion chamber. Although all cases originate from the same injection stagnation pressure, configurations with larger imposed heat addition exhibit a progressively larger cumulative pressure deficit at the combustor exit. Conversely, reduced heat addition yields a smaller overall stagnation pressure loss. The separation between curves increases continuously in the downstream direction, demonstrating that Rayleigh losses accumulate spatially as entropy is generated throughout the chamber length.

This behavior directly illustrates the central mechanism investigated in this study: heat addition within a constant-area compressible flow irreversibly reduces stagnation pressure prior to nozzle expansion. Because nozzle performance depends on the available stagnation pressure at its inlet, reductions incurred within the combustion chamber directly limit the expansion work that can be extracted downstream. Consequently, even modest increases in total temperature rise produce measurable decreases in exit stagnation pressure, which propagate through the expansion process and affect thrust and specific impulse, as discussed in the subsequent sections.

C. Rayleigh Loss Evaluation

To quantify the cumulative impact of heat addition on available stagnation pressure, the nozzle exit stagnation pressure was normalized by the injection face stagnation pressure. Figure 5 presents the results for the stagnation pressure ratio evaluated across the total temperature sweep.

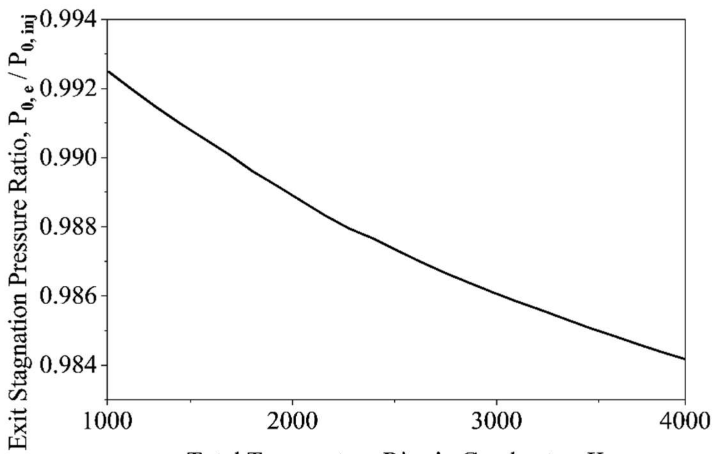

Fig. 5 Ratio of Nozzle Exit Stagnation Pressure to Initial Stagnation Pressure, Plotted vs. Total Temperature Increase in Combustion Chamber

The exit stagnation pressure ratio decreases monotonically with increasing total temperature rise, demonstrating that intensified heating in the combustion chamber produces progressively larger entropy-driven pressure degradation across the entire thrust chamber. Although the total pressure ratios are modest in absolute magnitude, the trend is systematic and fully consistent with classical Rayleigh flow behavior, in which subsonic heat addition drives a reduction in stagnation pressure due to irreversible entropy generation. As the imposed total temperature rise increases, the cumulative thermodynamic penalty compounds axially, resulting in a measurable reduction in the stagnation pressure available at the nozzle exit for expansion. Because all cases begin at identical injection face stagnation pressure and share identical geometry and friction modeling, the observed reduction in the ratio directly isolates the thermodynamic consequences of heat addition alone. This controlled comparison confirms that the degradation is not a geometric or viscous artifact, but rather a direct production of Rayleigh losses within the combustor.

To directly characterize Rayleigh stagnation pressure losses, the loss metric defined in Eq. (10) was evaluated at the combustor exit across the full total temperature sweep. Figure 6 presents the resulting Rayleigh total pressure loss expressed as a percentage of the ideal reference case where no losses occur.

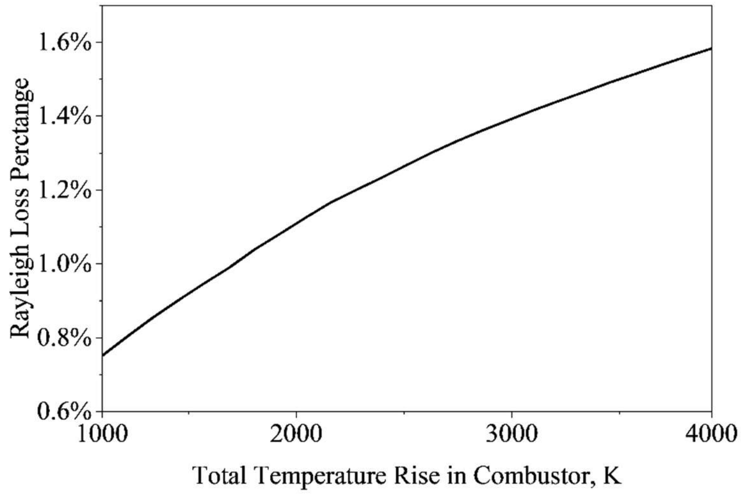

Fig. 6 Percent Rayleigh Loss in Stagnation Pressure, Plotted versus Total Temperature Increase in Combustion Chamber

The Rayleigh loss percentage increases nonlinearly with increasing total temperature rise, indicating that stagnation pressure losses are sensitive to heat addition at elevated temperature rise levels. This behavior arises from the coupled dependence of entropy generation on both the imposed total temperature gradient and the evolving thermodynamic properties of the propellants. These results establish a direct quantitative relationship between heat addition and available stagnation pressure prior to nozzle expansion, forming the foundation for the performance trends examined in the following section.

D. Performance Trends

The performance impact of Rayleigh-induced stagnation pressure degradation was quantified by evaluating thrust loss and specific impulse loss as a function of prescribed total temperature rise. Figure 7 presents the percent reduction in thrust and specific impulse relative to the corresponding ideal reference solution across the investigated temperature range.

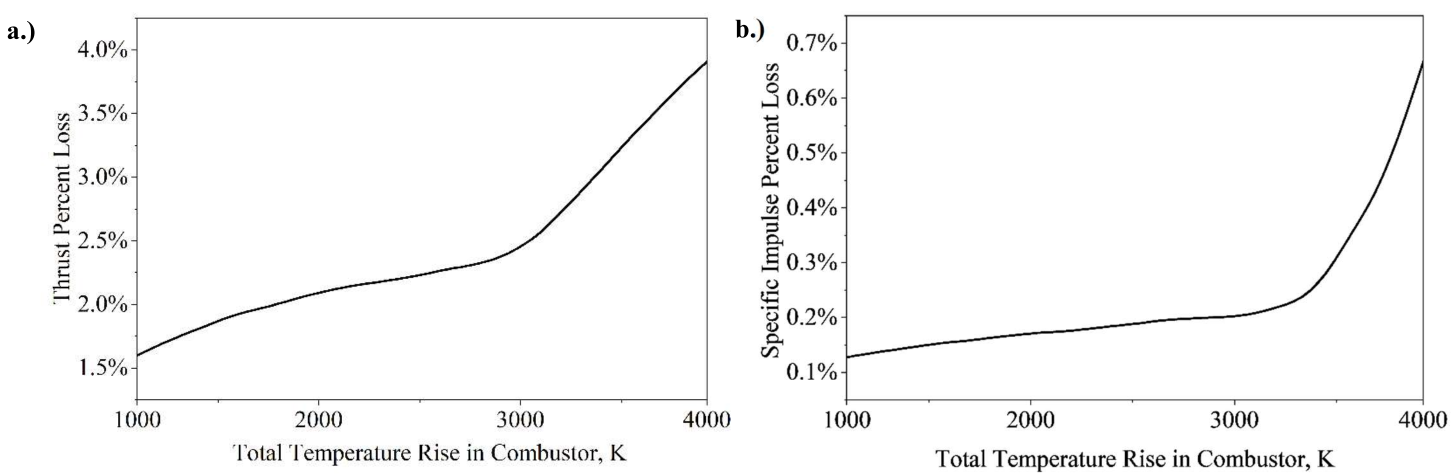

Fig. 7 Percent Loss in Performance Metrics: (a) Thrust, (b) Specific Impulse, Plotted versus Total Temperature Increase in Combustion Chamber

Thrust loss increases monotonically with total temperature rise, growing from approximately 1.6% at the lower bound of the sweep to nearly 4% at the highest total temperature increase. The trend exhibits a gradual increase at moderate temperature levels, followed by a more pronounced rise beyond approximately 3000 K. This behavior reflects the nonlinear sensitivity of stagnation pressure degradation to intensified heat addition. As entropy generation within the combustion chamber increases, the available stagnation pressure at the nozzle inlet decreases, reducing momentum thrust and amplifying overall performance losses.

Specific impulse loss follows a similar trend but remains smaller in magnitude, increasing from approximately 0.13% to roughly 0.65% across the temperature sweep. Because specific impulse normalizes thrust by mass flow rate, its comparatively smaller degradation indicates that a portion of the thrust reduction is associated with variations in mass flow rate in addition to stagnation pressure losses. The nonlinear increase at elevated temperature increase levels again highlights the compounded thermodynamic impact of Rayleigh heat addition.

These results demonstrate that even modest stagnation pressure degradation within the combustion chamber propagates through the expansion process to produce measurable reductions in engine-level performance.

V. Conclusion

High fidelity numerical methods capable of resolving combustion chamber thermodynamics are computationally expensive and often impractical for rapid early-stage trade studies. This work presents a computationally efficient quasi-one-dimensional framework for reconstructing stagnation pressure evolution in LPREs and isolating Rayleigh total pressure losses attributable solely to heat addition within the combustion chamber. Frictional effects are retained in the Mach number solution to preserve realistic flow development, but entropy reconstruction excludes frictional contributions to quantify stagnation pressure decay induced from heat addition independently. A systematic sweep of combustion chamber total temperature rise is performed for a fixed engine geometry, and performance impacts are evaluated relative to a constant stagnation pressure baseline.

Results demonstrate a monotonic decrease in stagnation pressure with increasing total temperature rise, leading directly to measurable reductions in thrust and specific impulse. These findings emphasize that Rayleigh losses introduce a non-negligible thermodynamic penalty even when geometric and frictional parameters are held constant. The sensitivity trends observed highlight the importance of explicitly modeling combustion induced stagnation pressure degradation during early-stage internal ballistics analysis.

Validation against NASA CEA shows good agreement in exit pressure and overall performance metrics, supporting the physical consistency of the approach. Minor deviations are attributed to modeled friction and the quasi-one-dimensional assumptions inherent to the framework.

Although the present model assumes thermodynamic equilibrium and employs a prescribed stagnation temperature rise to represent combustion, it captures the primary physical mechanism governing Rayleigh pressure losses. Multidimensional effects, detailed injector-flow interactions, and shock structures are not resolved but represent logical extensions of this work. Future developments may include direct coupling with finite-rate chemistry solvers, incorporation of injector pressure drop modeling, and refinement of geometric representations to further enhance predictive capability. Overall, the presented framework provides a physically grounded and computationally efficient tool for evaluation of Rayleigh loss sensitivity in LPRE internal ballistics and supports informed performance trade studies without the expense of high-fidelity simulation.

VI. References

[1] Huzel, Dieter K. and Huang, David H., Design of Liquid Propellant Rocket Engines, Rocketdyne Division, North American Rockwell, Inc, Washington, D.C., 1971 (updated version currently published by AIAA)

[2] Sutton, G. P., and Biblarz, O., *Rocket Propulsion Elements*, 9th ed., John Wiley & Sons Inc., Hoboken, New Jersey, 2017.

[3] Anderson, J. D., Jr. (2003). *Modern Compressible Flow with Historical Perspective* (3rd ed.). McGraw-Hill.

[4] Gordon, S., and McBride, B. J., "Computer Program for Calculation of Complex Chemical Equilibrium Compositions and Applications," NASA Reference Publication 1311, 1996.

[5] Shapiro, Ascher H., *The Dynamics and Thermodynamics of Compressible Fluid Flow*, John Wiley and Sons, 1953.

[6] Hill, P., and Peterson, C., *Mechanics and Thermodynamics of Propulsion*, Addison Wesley, 1992.

[7] Mattingly, *Elements of Gas Turbine Propulsion*. AIAA, 2006.

[8] Anderson, John D., *Hypersonic and High Temperature Gas Dynamics*, McGraw-Hill Book Company, 1989.